

## Heat Capacity and Thermodynamic Functions of $\text{MnCl}_2 \cdot 2\text{H}_2\text{O}$ and $\text{MnCl}_2 \cdot 2\text{D}_2\text{O}$

J. E. MOORE\* AND R. A. BUTERA†

*Department of Chemistry, University of Pittsburgh,  
Pittsburgh, Pennsylvania 15260*

Received March 21, 1985

The heat capacities of  $\text{MnCl}_2 \cdot 2\text{H}_2\text{O}$  and  $\text{MnCl}_2 \cdot 2\text{D}_2\text{O}$  have been experimentally determined from 1.4 to 300 K. The smooth heat capacity and the thermodynamic functions ( $H_T^\circ - H_0^\circ$ ) and  $S_T^\circ$  are reported for the two compounds over the 10 and 300 K temperature range. The error in the thermodynamic functions at 10 K is estimated at 3%. Additional error in the tabulated values arising from the heat capacity data above 10 K is thought to be less than 1%. Lambda-shaped heat capacity features associated with antiferromagnetic ordering were observed at  $6.67 \pm 0.08$  and  $6.61 \pm 0.08$  K for the dihydrate and dideuterate, respectively. In addition, compound heat capacity anomalies consisting of a small lambda-shaped feature at  $57.7 \pm 0.5$  K with a comparably large high-temperature shoulder extending to approximately 70 K were observed in both the dihydrate and dideuterate. The entropies associated with these anomalies are  $0.42 \pm 0.04$  and  $1.04 \pm 0.04$  J/mole-K, respectively. © 1986 Academic Press, Inc.

### Introduction

The prior interest in manganese chloride dihydrate has been diverse. Previous work has included study of the antiferromagnetic ordering which occurs at approximately 6.7 K (1-4), the crystal structure and the hydrogen-bonded environment (5-7), and the electronic states of the divalent manganese ion (8, 9).

The work reported here is an outgrowth of an ongoing study of the manganese halide tetrahydrate and tetradeuterate systems. In regard to the tetrahydrates and tetradeuterates, the dihydrates and dideuterates can be contaminants arising

\* Present address: AT&T Bell Laboratories, Murray Hill, N.J. 07974.

† For all correspondence.

from surface dehydration. The initial intent of the present study was to accurately determine the heat capacity behavior of the dihydrates and dideuterates in order to identify any anomalous heat capacity features which might be attributable to these lower hydrates and deuterates. In addition to the expected heat capacity features associated with the antiferromagnetic ordering, mid-temperature heat capacity anomalies were observed. These anomalies are thought to be associated with hydrogen and deuterium bond ordering.

The purpose of the present paper is to report the smooth heat capacity and the thermodynamic functions ( $H_T^\circ - H_0^\circ$ ) and  $S_T^\circ$  for  $\text{MnCl}_2 \cdot 2\text{H}_2\text{O}$  and  $\text{MnCl}_2 \cdot 2\text{D}_2\text{O}$  over the 10 to 300 K temperature range. The tabulated values are derived from calorimetric

measurements performed over the 1.4 to 300 K temperature range.

### Sample Preparations

Manganese chloride  $\text{H}_2\text{O}$  and  $\text{D}_2\text{O}$  solutions were prepared by direct reaction of manganese metal (Puratronic grade 1 manganese flake, Johnson Matthey Chemicals Ltd., Orachard Rd., Royston Herts, SG8 5HE, England; distributed by Alpha Products, Danvers, Mass. 01923) with concentrated aqueous hydrogen chloride (ACS Reagent grade, Fisher Scientific Co., Fairlawn, N.J. 07410) and deuterium chloride in  $\text{D}_2\text{O}$  (Deuterium chloride, 37 wt% solution in  $\text{D}_2\text{O}$  99 atom.% D, Aldrich Chemical Co., Milwaukee, Wisc. 53233), respectively. In the case of the deuterated compound, the reaction and all subsequent manipulations were carried out in a glove bag under an inert atmosphere. The solutions were crystallized at  $70^\circ\text{C}$  inside desiccators with molecular sieves serving as the desiccant. The crystals obtained displayed the characteristic dihydrate morphology (5), and were 1 to 2 mm in diameter and up to 3 cm long. The previously reported problems of occluded solution and resultant tetrahydrate/tetradewater contamination

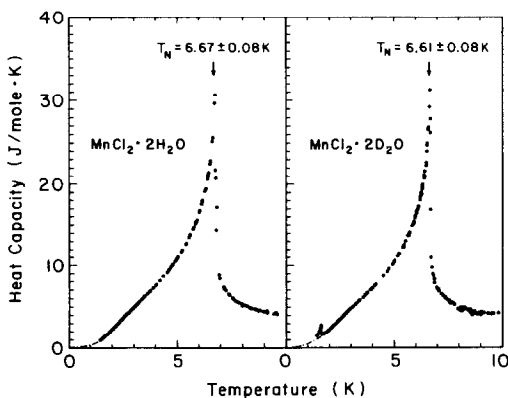


FIG. 1. Experimental heat capacity data for  $\text{MnCl}_2 \cdot 2\text{H}_2\text{O}$  and  $\text{MnCl}_2 \cdot 2\text{D}_2\text{O}$  below 10 K.

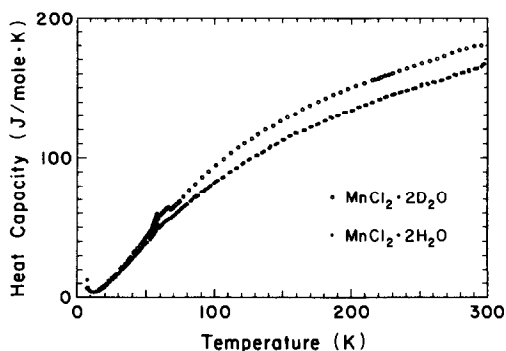


FIG. 2. Experimental heat capacity data for  $\text{MnCl}_2 \cdot 2\text{H}_2\text{O}$  and  $\text{MnCl}_2 \cdot 2\text{D}_2\text{O}$  above 10 K.

(4) were not found to be a serious difficulty, as evidenced by Fig. 1.

The  $\text{MnCl}_2 \cdot 2\text{D}_2\text{O}$  was found to be 94.9 atom.% D. The details of this assay procedure have been described elsewhere (10), though the essence of the procedure is to determine the atom.% H concentration in a  $\text{D}_2\text{O}$  sample using proton NMR with an internal standard peak (DMSO). The  $\text{D}_2\text{O}$  sample is obtained by "distilling" the waters of deuteration from a crystalline sample of the deuterated material into a tared NMR tube. The assay was performed after the calorimetric measurements were completed, and represents an upper limit of the hydrogen contamination of the sample.

### Apparatus

Two calorimeters were used in this study. The adiabatic calorimeter which was used for temperatures above 10 K has been described elsewhere (11, 12). The sample sizes used in this calorimeter were 27 and 19 g of the dihydrate and dideuterate, respectively. The accuracy of the data obtained from this instrument is expected to be within 1%.

For temperatures below 10 K, a pulse calorimeter was used. A brief description of this calorimeter has been given (10), and a more complete description is in preparation. The calorimeter is run in a quasi-

isothermal mode, and the sample sizes used in the present work were approximately 50 mg. The data obtained from this calorimeter are expected to be accurate to about 3%. Design modifications to improve the accuracy to within 1% are presently underway.

## Results and Discussion

Figure 1 shows the experimental heat capacity data<sup>1</sup> for temperatures below 10 K. The dot-dashed lines from the low-temperature limits of the data to 0 K are the extrapolations used to reference the thermodynamic functions to absolute zero. In the case of the dideuterate, the small feature at 1.6 K indicates the presence of some  $\text{MnCl}_2 \cdot 4\text{D}_2\text{O}$  contamination. The heat capacity behavior of the dihydrate was used to undercut the heat capacity contribution from the antiferromagnetic ordering of the tetra-deuterate contamination. Based on the entropy content of the extracted feature, the  $\text{MnCl}_2 \cdot 4\text{D}_2\text{O}$  contamination was much less than 1% by mass.

Although the absolute accuracy of the inferred Neel temperatures is conservatively estimated to be within 80 mK, the precision of the temperature measurements and the heat capacity data is greater (i.e., the data shown in Fig. 1 for  $\text{MnCl}_2 \cdot 2\text{H}_2\text{O}$  are the composite of two separate calorimeter samples with heat capacity measurements made over the entire 1.4 to 10 K range in each case).

<sup>1</sup> See NAPS document No. 04357 and 51 pages of supplementary material. Order from ASIS/NAPS, Microfiche Publications, P.O. Box 3513, Grand Central Station, New York, NY 10163. Remit in advance \$4.00 for microfiche copy or for photocopy, \$7.75 up to 20 pages plus \$0.30 for each additional page. All orders must be prepaid. Institutions and organizations may order by purchase order. However, there is a billing and handling charge for this service of \$15. Foreign orders add \$4.50 for postage and handling, for the first 20 pages, and \$1.00 for additional 10 pages of material. Remit \$1.50 for postage of any microfiche orders.

The Neel point at  $6.67 \pm 0.08$  K is in good agreement with the 6.68 K value obtained in previous heat capacity measurements (3), but is in somewhat poorer agreement with the values of 6.8 and 6.90 K derived from NMR (1) and susceptibility (4) measurements, respectively. From the data of Fig. 1, the shift in Neel point with deuteration is found to be  $-0.90\%$ . This result follows the trend found for other manganese halide hydrates and their corresponding deuterates (10, 11, 13).

Figure 2 shows the experimental heat capacity data<sup>1</sup> for temperatures above 10 K. Both of the compounds display mid-temperature heat capacity anomalies.

Our method of smoothing the experimental data involves the use of a draftsman's spline, and has been detailed elsewhere (11). Figures 3 and 4 show the percentage deviation between the experimental data and the smooth heat capacity curves for the two compounds. For these plots, the  $\Delta\%$  is given by

$$\Delta\%C_p = \frac{\text{Smooth } C_p - \text{Experimental } C_p}{\text{Smooth } C_p} \cdot 100\%.$$

The enhanced scatter over the 50 to 80 K temperature range is attributed to the use of small-temperature-step sizes in the heat capacity measurements. These small-temper-

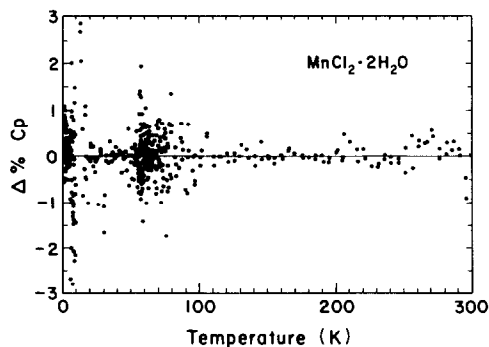


FIG. 3. Percentage deviation between smoothed and experimental heat capacity data for  $\text{MnCl}_2 \cdot 2\text{H}_2\text{O}$ .

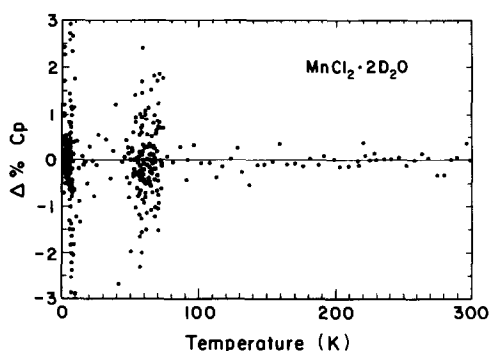


FIG. 4. Percentage deviation between smoothed and experimental heat capacity data for  $\text{MnCl}_2 \cdot 2\text{D}_2\text{O}$ .

ature-step sizes are required to resolve the shape of the heat capacity anomalies, but are less accurate and display an increased degree of scatter.

Tables I and II give the smooth heat capacity and the thermodynamic functions ( $H_T^\circ - H_0^\circ$ ) and  $S_T^\circ$  for  $\text{MnCl}_2 \cdot 2\text{H}_2\text{O}$  and  $\text{MnCl}_2 \cdot 2\text{D}_2\text{O}$ , respectively. The error in the thermodynamic functions at 10 K is thought to be less than 1%. The thermodynamic functions were obtained numerically from the smooth heat capacity. The data density used in these evaluations was much greater than reported here, and the error associated with the numerical treatment is insignificant.

Figure 5 shows the mid-temperature anomalies for the two compounds in detail. For these plots, the data are plotted as bars indicating the initial and final temperatures of the individual heat capacity measurements. The dot-dashed lines are estimated blank heat capacity curves. These curves are based on 6th-order polynomial least-squares fits to the smooth heat capacity data adjacent to the anomaly regions (11). Although the sharp lambda-shaped features appear to occur at the same temperature, the entropy content of the two anomalies is quite different. From the estimated blank curves, the entropies are found to be  $0.42 \pm 0.04$  and  $1.04 \pm 0.04$  J/mole-K for  $\text{MnCl}_2 \cdot$

$2\text{H}_2\text{O}$  and  $\text{MnCl}_2 \cdot 2\text{D}_2\text{O}$ , respectively. In both cases, the high-temperature shoulder accounts for most of the entropy.

Lacking the results of microscopically

TABLE I  
SMOOTH THERMODYNAMIC FUNCTIONS  
FOR  $\text{MnCl}_2 \cdot 2\text{H}_2\text{O}$

$T$ (K)	$C_p$ (J/mole-K)	$H_T^\circ - H_0^\circ$ (J/mole)	$S_T^\circ$ (J/mole-K)
10.00	4.15	68.42	13.39
15.00	4.70	88.60	15.02
20.00	7.91	119.46	16.77
25.00	12.21	169.49	18.99
30.00	17.15	242.63	21.64
35.00	22.47	341.59	24.68
40.00	27.91	467.60	28.04
45.00	33.43	620.93	31.64
50.00	38.71	801.57	35.44
55.00	44.68	1009.07	39.39
60.00	51.19	1251.96	43.62
65.00	55.51	1520.35	47.91
70.00	58.58	1803.35	52.10
75.00	62.79	2106.64	56.29
80.00	67.07	2431.18	60.48
85.00	71.39	2777.47	64.67
90.00	75.42	3144.60	68.87
95.00	79.05	3531.02	73.05
100.00	82.52	3934.99	77.19
110.00	89.12	4793.41	85.37
120.00	95.42	5716.25	93.39
130.00	101.43	6700.78	101.27
140.00	107.15	7743.89	109.00
150.00	112.44	8842.23	116.57
160.00	117.27	999.114	123.99
170.00	121.76	11186.52	131.23
180.00	126.11	12425.96	138.31
190.00	130.26	13707.97	145.25
200.00	134.20	15030.55	152.03
210.00	137.85	16390.91	158.66
220.00	141.35	17787.15	165.16
230.00	144.73	19217.79	171.52
240.00	147.92	20681.10	177.75
250.00	151.09	22176.14	183.85
260.00	154.20	23702.58	189.83
270.00	157.30	25260.08	195.71
273.15	158.26	25757.09	197.54
280.00	160.35	26848.32	201.49
290.00	163.42	28467.19	207.17
298.15	165.90	29809.18	211.73
300.00	166.47	30116.62	212.76

TABLE II  
SMOOTH THERMODYNAMIC FUNCTIONS FOR  
 $\text{MnCl}_2 \cdot 2\text{D}_2\text{O}$

$T$ (K)	$C_p$ (J/mole-K)	$H_T^\circ - H_0^\circ$ (J/mole)	$S_T^\circ$ (J/mole-K)
10.00	3.87	65.13	13.05
15.00	5.05	85.45	14.68
20.00	8.51	118.87	16.58
25.00	13.18	172.64	18.96
30.00	18.52	251.72	21.83
35.00	24.15	358.35	25.10
40.00	29.91	493.42	28.70
45.00	35.91	657.81	32.57
50.00	42.39	853.36	36.68
55.00	49.81	1082.90	41.05
60.00	57.59	1356.25	45.81
65.00	63.44	1659.33	50.65
70.00	64.20	1977.49	55.37
75.00	69.60	2312.05	59.99
80.00	74.84	2673.22	64.64
85.00	79.92	3060.17	69.33
90.00	84.55	3471.47	74.03
95.00	88.97	3905.34	78.73
100.00	93.17	4360.79	83.40
110.00	100.97	5332.16	92.65
120.00	108.05	6377.82	101.74
130.00	114.62	7491.58	110.65
140.00	120.73	8668.63	119.37
150.00	126.44	9904.87	127.90
160.00	131.77	11196.28	136.23
170.00	136.67	12538.95	144.37
180.00	141.25	13928.82	152.32
190.00	145.42	15362.52	160.07
200.00	149.24	16836.04	167.62
210.00	152.90	18346.95	174.99
220.00	156.35	19893.39	182.19
230.00	159.70	21473.76	189.21
240.00	162.94	23086.99	196.08
250.00	166.12	24732.29	202.79
260.00	169.27	26409.20	209.37
270.00	172.42	28117.64	215.82
273.15	173.41	28662.33	217.82
280.00	175.58	29857.57	222.14
290.00	178.68	31628.94	228.36
298.15	181.20	33095.54	233.35
300.00	181.77	33431.28	234.47

sensitive measurements over the anomaly regions, we hesitate to make any definitive statements concerning the processes responsible for the observed features. Based on the crystal structure, it is tempting to

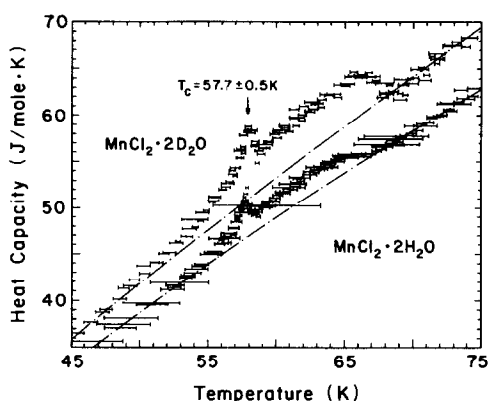


FIG. 5. Heat capacity anomalies in  $\text{MnCl}_2 \cdot 2\text{H}_2\text{O}$  and  $\text{MnCl}_2 \cdot 2\text{D}_2\text{O}$ .

conclude that a hydrogen/deuterium bond order-disorder transition is involved. A small mole-fraction of disorder in the ideal hydrogen bonding scheme (5, 6) could account for the observed anomaly entropies, however the possible arguments for the unusual anomaly shapes are still highly speculative.

A very useful study in regard to elucidating the processes involved would be an IR profile measurement of the hydrogen modes as a function of temperature across the transition region. If there is disorder in the hydrogen-bonded structure above the transition temperature, the line profiles should reflect this in the form of inhomogeneous broadening. A marked decrease in the profile width below the transition region could be interpreted in favor of the hydrogen bond order-disorder proposal.

### Acknowledgment

One of the authors (J.E.M.) would like to thank the Andrew Mellon Foundation for its support in the form of a predoctoral fellowship.

### References

1. R. D. SPENCE AND K. V. S. R. RAO, *J. Chem. Phys.* **52**, 2740 (1970).

2. T. GOTO, A. HIRAI, AND T. HASEDA, *Phys. Lett.* **33A**, 185 (1970).
3. P. T. BAILEY, J. R. RICKS, AND H. FORSTAT, *Bull. Amer. Phys. Soc.* **14**, 540 (1969).
4. J. N. MCELEARNEY, S. MERCHANT, AND R. L. CARLIN, *Inorg. Chem.* **12**, 906 (1973).
5. B. MOROSIN AND E. J. GRAEBER, *J. Chem. Phys.* **42**, 898 (1965).
6. Z. W. EL SAFFAR, *J. Chem. Phys.* **52**, 4097 (1970).
7. R. A. FIFER AND J. SCHIFFER, *J. Chem. Phys.* **52**, 2664 (1970).
8. D. H. GOODE, *J. Chem. Phys.* **43**, 2830 (1965).
9. K. E. LAWSON, *J. Chem. Phys.* **44**, 4159 (1966).
10. J. E. MOORE AND R. A. BUTERA **60**, 88 (1985).
11. J. E. MOORE AND R. A. BUTERA, *J. Solid State Chem.* **59**, 81 (1985).
12. D. J. GERMANO, R. A. BUTERA, S. G. SANKAR, AND K. A. GSCHNEIDER, JR., *J. Appl. Phys.* **50**, 7495 (1979).
13. C. L. YUE AND B. G. TURRELL, *Solid State Commun.* **8**, 1261 (1970).